ELSEVIER

Nuclear Instruments and Methods in Physics Research B 160 (2000) 172–181

NIM B
Beam Interactions with Materials & Atoms

www.elsevier.nl/locate/nimb

Electric discharge of helium-filled proportional counter at liquid helium temperature

Sei Masaoka [a], Rintaro Katano [a], Yasuhito Isozumi [b,*]

[a] *Institute for Chemical Research, Kyoto University, Uji, Kyoto 611-0011, Japan*
[b] *Radioisotope Research Center, Kyoto University, Kyoto 606-8501, Japan*

Received 3 May 1999; received in revised form 1 July 1999

Abstract

In the present work the electric discharge of the helium-filled proportional counter (HFPC) at liquid helium temperature (4.2 K), which is used as an electron detector in the cryogenic resonance-electron Mössbauer spectroscopy has been studied both experimentally and theoretically. The analysis for observed discharge current has revealed that non-resonance radiations from excited helium atoms, which are created in electron avalanches near the anode, play a dominant role to initiate the electric discharge. A theoretical treatment for the current multiplication in discharge is also described.

Keywords: Electric discharge; Helium-filled counter; Liquid helium

1. Introduction

Resonance-electron Mössbauer spectroscopy (REMS) or conversion-electron Mössbauer spectroscopy (CEMS) is one of the important methods for the study of surface layer of metals, alloys and chemical compounds including iron, tin and europium [1–4]. The helium-filled proportional counter (HFPC) is often applied to detect electrons resonantly scattered from samples in the REMS measurement performed at low temperatures near 4.2 K [3–7]. A main feature of HFPC is that its proportional region is very narrow; the available maximum gas gain is the order of 10^2 at the low temperatures [8–10]. The operation with higher gas gains is limited by the self-sustained electric discharge, which is always initiated at a certain threshold of anode voltage depending on density and temperature of helium gas.

A systematic investigation on the electric discharge is clearly necessary to understand more in detail the operation of HFPC and to develop a new HFPC with gas gains higher than 10^2, if possible. We report here some results obtained by our recent study on the electric discharge in HFPC. In Section 2, some prior knowledge on the

* Corresponding author. Tel.: +81-75-753-7512; fax: +81-75-753-7504.
E-mail address: yasuhito@barium.rirc.kyoto-u.ac.jp (Y. Isozumi)

0168-583X/00/$ - see front matter
PII: S0168-583X(99)00547-9

discharge are given to explain the motivation of the present work. In Section 3, the experimental procedure to observe the electric discharge is described in brief. The method to analyze the discharge signal and experimental results are given in Section 4. A theoretical treatment for the discharge and comparison between experiment and theory are given in Section 5. The mechanism of the discharge is discussed in Section 6. Some future works are suggested in Section 7.

2. Condition of electric discharge

Many active particles such as photons, positive ions and metastables are produced in electron avalanches near the anode wire. When a part of such particles collides with a cathode material, electrons are emitted with a certain probability. These secondary electrons drift to the anode and there induce new electron avalanches. Therefore, the number of electron avalanches is successively increased if the number of secondary electrons emitted from the cathode is larger than unit per avalanche. This process is called current multiplication in electric discharge.

In the present case with helium gas at normal condition, i.e., 760 Torr at room temperature, most of the helium metastables, $He^m(2^1s)$ and $He^m(2^3s)$, are de-excited to the ground state by colliding with normal helium atoms He (1^1s). Therefore, the contribution of the metastables to the secondary electron emission is negligibly small.

Thus, a condition to bring out the current multiplication is given by

$$R_p + R_i > 1. \tag{1}$$

In the above expression, R_p is defined as the number of secondary electrons per avalanche, which are emitted through the collision of the active photons with cathode materials. This parameter is related to the second Townsend ionization coefficient of the photons Γ_p, i.e., a probability with which an active photon emits an electron through the collision with cathode [11]:

$$R_p = N_p \Gamma_p, \tag{2}$$

where N_p is the number of the active photons per avalanche. For the positive ions, we obtain

$$R_i = N_i \Gamma_i, \tag{3}$$

where R_i, N_i and Γ_i are defined similarly to R_p, N_p and Γ_p, respectively.

At room temperature, a counter filled with pure helium gas does not operate in the proportional region with enough gas gains. Helium ions, He^+, produced in an electron avalanche are immediately changed to molecular helium ions He_2^+. The ionization coefficient Γ_i for He_2^+ is 0.13 at room temperature [12]. This value is so large as to generate the electric discharge at gas gains near 10. Positive helium ion clusters He_n^+ $(n > 10)$ are formed in the drift of He_2^+ from anode to cathode at low temperatures near 4.2 K; the coefficient Γ_i is decreased to $\sim 10^{-3}$ by the formation of the cluster ions at the low temperatures [10]. This is a main reason why HFPC operates at the low temperatures.

Since almost all positive ions created in an avalanche arrive at the cathode, an average of N_i in Eq. (3) nearly equals to the gas gain G. If the electric discharge at the low temperatures is caused by the positive ion clusters, i.e., $R_i > 1$, the maximum gas gain $G_{max}(> 1/\Gamma_i)$ is of the order of 10^3. On the contrary, our previous experiments indicate that G_{max} is near 10^2 [8–10]. This strongly implies that the secondary electron emission in HFPC is caused not only by the positive helium ions but also the contribution from the active photons is to be taken into consideration. The motivation of the present work is to make clear the role of the active photons in the electric discharge of HFPC.

3. Experiment

A layout of HFPC is shown in Fig. 1. The anode (A) is a 30-μm diameter gold-plated tungsten wire and the cathode (CA) is a 25-mm diameter × 76-mm long stainless steel pipe. In order to lower the distortion of the electric field inside the counter, field tubes (FT, 1-mm diameter × 7-mm length) are mounted at both ends of the anode. The high voltage is fed into the anode through a glass feed through (G). Insulators (I) between the

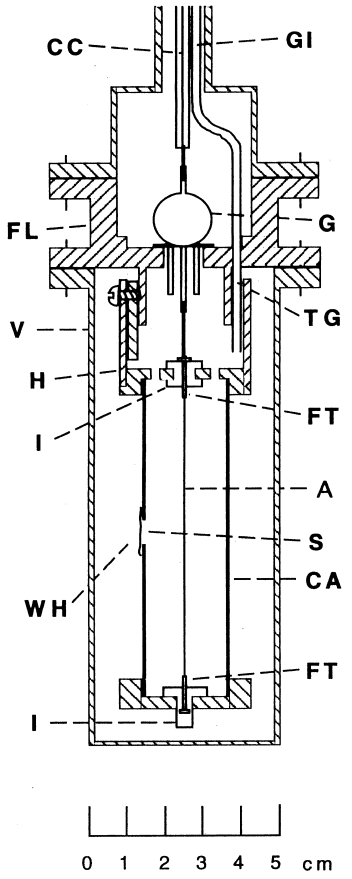

Fig. 1. Layout of the helium-filled proportional counter: A, anode (30-μm diameter gold-plated tungsten wire); CA, cathode (25-mm diameter × 76-mm long stainless steel pipe); WH, 8-mm diameter hole in the cathode cylinder; S, ^{210}Po source on 20-μm thick aluminum foil; FT, field tube; G, glass feedthrough; I, Teflon insulator; H, aluminum holder; V, stainless steel vessel; GI, gas inlet (3-mm diameter stainless steel pipe); FL, brass flange; CC, coaxial cable.

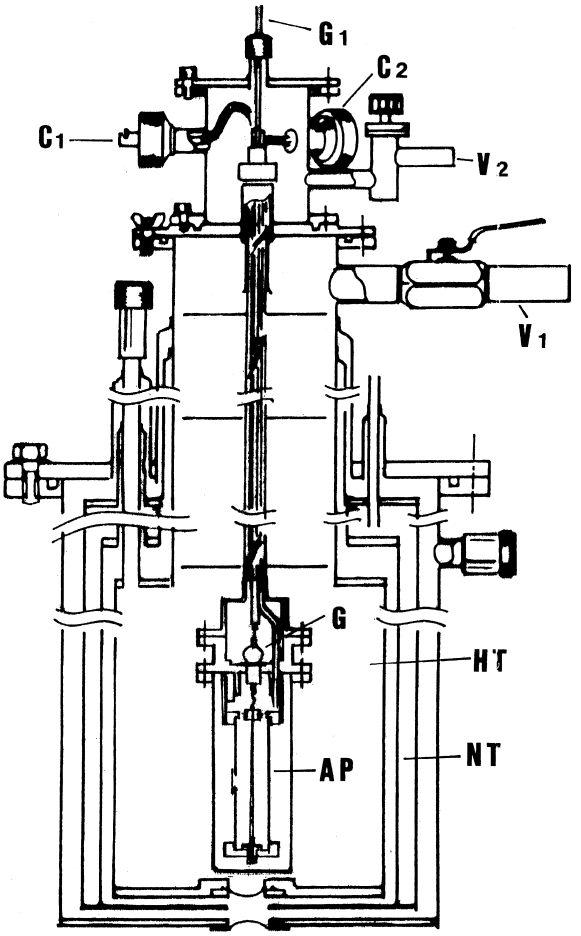

Fig. 2. Layout of the cryostat to mount the helium-filled proportional counter: GI, gas inlet; C1, connector assembly to pick up radiation signals; C2, connecter assembly for thermocouple and others; V1, valve for helium pumping; V2, vacuum valve; HT, liquid helium tank; NT, liquid nitrogen tank; G, glass feedthrough; AP, helium-filled proportional counter.

anode and the cathode are made of Teflon. The counter is fixed on a flange (FL) by an aluminum holder (H) and put in a stainless steel vessel (V) sealed by an indium wire. The signal cable (CC) consists of a copper wire (0.2-mm diameter), a Teflon pipe (3.0-mm outer diameter and 0.5-mm thickness) and a stainless steel pipe (4.0-mm diameter and 0.5-mm thickness). The length of the cable is about 1 m and its capacitance is about 50 pF. The preamplifier used is a commercially available one, CANBERRA 2003T, of which the nominal noise (FWHM, Si) is 2.0 keV with no capacitance and the decay time constant is 250 μs. The counter assembly is mounted at the bottom of a cryostat, as shown in Fig. 2. The counter and the vessel (V) in Fig. 1 were cleaned with acetone and ethanol in an ultrasonic washer, and then evacuated to 10^{-5}–10^{-6} Torr for about 10 h. Impurities in helium, e.g., water, were carefully adsorbed by molecular sieves which were cooled at liquid nitrogen temperature. Through a 3-mm diameter stainless steel pipe (GI in Figs. 1 and 2), the purified helium was introduced in HFPC at normal condition, i.e., with a pressure of 760 Torr at room

temperature (300 K). After sealing a small valve at the top of the pipe GI, the HFPC was cooled down to liquid helium temperature (4.2 K) by filling the tank HT (in Fig. 2) with liquid helium. The gas density of helium in the HFPC is estimated to be 2.45×10^{19} cm^{-3} in the present work.

The energy of α particles from ^{210}Po is 5.3 MeV. An α source was prepared by electroplating ^{210}Po on an aluminum foil with a thickness of 20 μm and a diameter of 25 mm; the radioactive area is in a diameter of 5 mm at the center of the foil and the intensity is ~ 10 Bq. The 10-mm diameter hole (WH in Fig. 1) at the middle of the cathode cylinder was covered with the source foil, of which the active surface looked inside the cylinder. The pulse rate of the α particles was about 2–3 s^{-1}. The range of 5.3 MeV α rays is 20.8 cm at the normal condition of helium gas. The energy loss of α particles in the helium gas layer of 2.5 cm, which equals to the diameter of HFPC, is about 0.63 MeV. This energy is high enough to detect without the gas amplification of HFPC, i.e., $G = 1$.

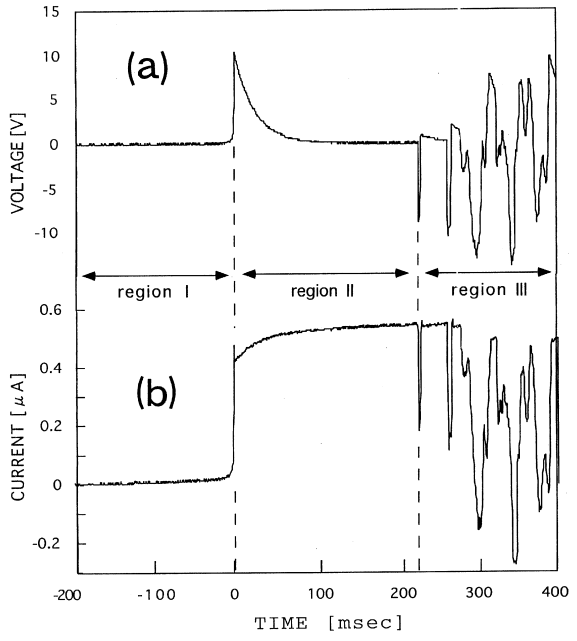

Fig. 3. Voltage and current signals of electric discharge: (a) discharge signal observed with the charge-sensitive preamplifier; (b) discharge current from HFPC, which is deduced from the discharge signal using the approximate transfer function of the preamplifier.

The voltage signal of the electric discharge observed with the preamplifier is given by Fig. 3(a). This discharge always takes place when the anode voltage becomes higher than a threshold value, 1200 V in the present case. The discharge cannot be suppressed unless the anode voltage is decreased down below 500 V. The output current from HFPC, rather than the output voltage from preamplifier, is necessary to examine the electric discharge directly. The result for the output current is given by Fig. 3(b), which was deduced by the method explained in Section 4.

4. Analysis for the discharge signal

4.1. Transfer function of the preamplifier

The transfer function of the preamplifier can be obtained by examining its impulsive and indential responses [13]. The impulsive response of charge-sensitive preamplifier is defined as the voltage output when the delta-function current is fed into a preamplifier. Since the delta-function current is equivalent to the step-function voltage for the input of charge-sensitive preamplifier, the impulsive response was obtained by feeding the step-function voltage into a preamplifier. The impulsive response was found to be an exponential with a decay time of $\tau_1 = 269 \pm 11$ μs, which is consistent with the nominal value given by CANBERRA, i.e., 250 μs. According to the theory of Laplace transformation [13], the transfer function is given by

$$W(p;\ \text{impulsive}) = \frac{A}{p + 1/\tau_1}, \tag{4}$$

where A is a constant value.

The indential response is defined as the voltage output when the step-function current is fed into a preamplifier. The indential response was obtained by feeding a linearly increasing voltage into the preamplifier; note that the linearly increasing voltage is equivalent to the step-function current for the input of charge-sensitive preamplifier. The observed response was an exponential with a decay time of $\tau_2 = 19.3 \pm 1$ μs. The transfer function is then given by

$$W(p;\ \text{indential}) = \frac{Bp}{p + 1/\tau_2}, \tag{5}$$

where B is a constant value.

Eqs. (4) and (5) indicate that the preamplifier works as an integration circuit in the frequency region of $\omega \geqslant 1/\tau_1 (= 3700\ \text{s}^{-1})$ and as a differentiating circuit in the region of $\omega \geqslant 1/\tau_2 (= 52\ \text{s}^{-1})$, respectively. The approximate expression of the work function is given by a product of Eqs. (4) and (5):

$$\begin{aligned} W(p) &= W(p;\ \text{impulsive}) \cdot W(p;\ \text{indential}) \\ &= \frac{1}{C_\text{f}} \frac{1}{p + 1/\tau_1} \frac{p}{p + 1/\tau_2}, \end{aligned} \tag{6}$$

where C_f is the feed-back capacitance of the charge-sensitive preamplifier. A simplified circuit composition of the preamplifier is shown by Fig. 4. The constant term $(1/C_\text{f})$ in Eq. (6) is deduced from an additional condition; when p becomes large, $W(p)$ approaches to the transfer function of the feed-back circuit in the preamplifier, i.e.,

$$W(p \to \text{large}) \to \frac{1}{C_\text{f}} \frac{1}{p + 1/\tau_1}. \tag{7}$$

Note that Eq. (6) is an approximate form of the transfer function, which is not precise enough in the frequency region of $52 < \omega < 3700\ \text{s}^{-1}$.

4.2. Output current from HFPC

The Laplace transform of the output voltage from the preamplifier, $V(p)$, is given by

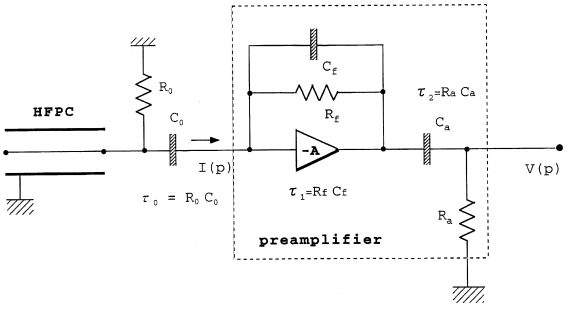

Fig. 4. A simplified circuit composition to deduce the approximate transfer function of the charge-sensitive preamplifier.

$$V(p) = W(p)I(p), \tag{8}$$

where $I(p)$ is the Laplace transform of the output current from HFPC. Using Eq. (8), $I(p)$ is deduced as

$$\begin{aligned} I(p) &= \frac{V(p)}{W(p)} \\ &= C_\text{f}\left[p + \left(\frac{1}{\tau_1} + \frac{1}{\tau_2}\right) + \frac{1}{\tau_1\tau_2}\frac{1}{p}\right] V(p). \end{aligned} \tag{9}$$

The output current $I(t)$ as a function of time is given by the inverse Laplace transformation of $I(p)$:

$$\begin{aligned} I(t) = C_\text{f}\Bigg[&\frac{\mathrm{d}V(t)}{\mathrm{d}t} + \left(\frac{1}{\tau_1} + \frac{1}{\tau_2}\right) V(t) \\ &+ \frac{1}{\tau_1\tau_2}\int_0^t V(s)\,\mathrm{d}s\Bigg]. \end{aligned} \tag{10}$$

Using Eq. (10), the discharge signal shown by Fig. 3(a) was transformed to the output current from HFPC, which is given by Fig. 3(b).

4.3. Gross structure of the discharge current

The output current $I(t)$ from HFPC can be divided into three regions as seen in Fig. 3(b). The current increases exponentially in region I and then discontinuously falls down. In region II, the current increases very gradually approaching to a constant level. After about 200 ms from the fall-down, the current repeats the steep fall-down and raise-up, as seen in region III. The current value becomes negative at some instances in this region. This inconsistency may be caused by the approximation in deducing the transfer function given by Eq. (6).

The exponential increase in region I is caused by the current multiplication, as discussed in Section 2. It is clear that relation (1) holds good in this region.

The number of electron avalanches on the anode wire keep increasing in the current multiplication process until the surface of anode is completely covered with avalanches. The output current is discontinuously decreased by the stop of the multiplication process, as seen at the end of region I. Then the current increases gradually by

adjusting the size and the surface density of avalanches on the anode. This adjustment results in an equilibrium current, which corresponds to an approaching constant current in region II.

The repetition of the steep fall-down and raise-up in region III has not been understood well in the present work. Helium gas in HFPC is warmed up by the comparatively large current in region II. The formation of molecular helium ion clusters He_n^+ is very sensitive to the temperature of helium gas. As the gas temperature is increased, the size n of ion clusters decreases. This results in the increase of the ionization coefficient Γ_i in Eq. (3). The behavior in the region III is probably caused by the rise of gas temperature.

4.4. Fit for the current multiplication curve

The curve shape of the current multiplication was determined by the non-linear least squares fit [14]. The best fit was obtained with two exponential components, as shown in Fig. 5; the increase of one component is much slower than that of other component. The result is expressed as

$$I(t) = A_s \exp(\lambda_s t) + A_f \exp(\lambda_f t). \quad (11)$$

The first term in the right side is the slow component of which parameters are given by

$$A_s = 0.16 \pm 0.01\ \mu A, \quad (12a)$$

$$\lambda_s = 0.68 \pm 0.02\ m\ s^{-1}. \quad (12b)$$

The second term is the fast component with

$$A_f = 0.12 \pm 0.01\ \mu A, \quad (13a)$$

$$\lambda_f = 8.13 \pm 0.01\ m\ s^{-1}. \quad (13b)$$

5. A theoretical treatment for the current multiplication

5.1. Formulation

The photons produced in the avalanche travel to the cathode in a very short time while the drift time of positive ions, T_i, to cathode is ~ 350 μs in the present case, as discussed later. The secondary electrons emitted from the cathode drift to the anode where they generate new electron avalanches; the drift time of electrons from the cathode to

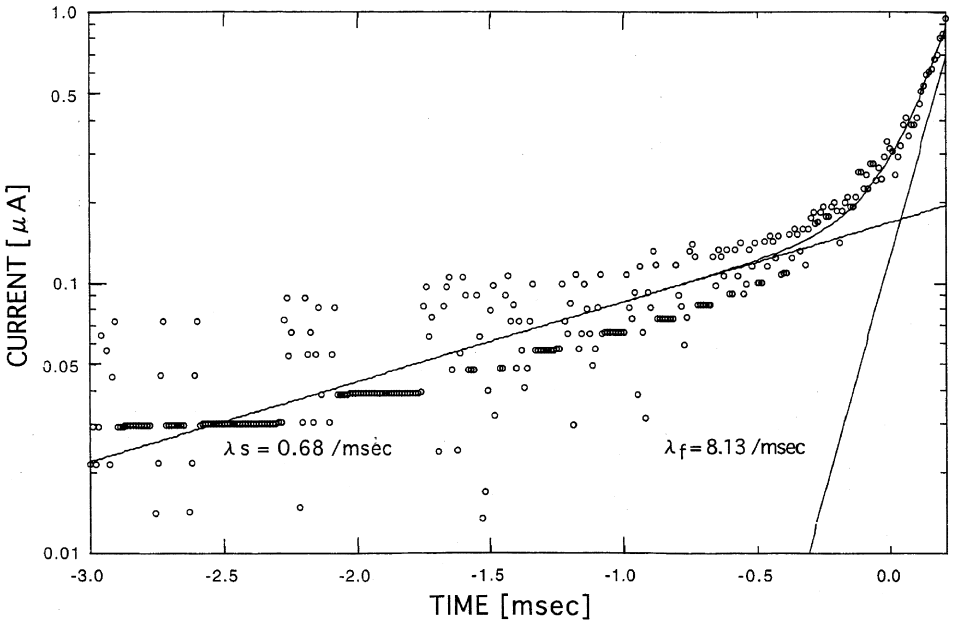

Fig. 5. The best fit for the current multiplication curve; the curve is resolved to two exponentials.

anode, T_e, is the order of 1 μs. Successive avalanches in the current multiplication take place as follows:

1. An avalanche with a size of G_0 is initiated at a time $t = 0$.
2. New avalanches with a size of $R_p G_0$ is generated by the photons at $t = T_e$ and the other new avalanches with the size of $R_i G_0$ is generated by the positive ions at $t = T_i$, where R_p and R_i are given by Eqs. (2) and (3), respectively.
3. After the avalanches produced by the process (2), new avalanches are successively generated; the avalanche caused by the photons has a size R_p time smaller and a time delay of $T_e(\sim \mu s)$ while that caused by the positive ions has a size R_i times smaller and a delay of $T_i(\sim \mu s)$.
4. The process (3) is repeated successively.

As seen in Appendix A, total charges produced in the current multiplication is expressed by

$$\Delta q(n,k) = eG_0 \sum_{s=0}^{n} R_i^s R_p^{(n-s)N_i+k} \binom{(n-s)N_i + k + s}{s}, \quad (14)$$

where

$$\binom{X}{x}$$

is the combination to select x from the ensemble X, e the charge of electron and n, k and N_i are defined in Appendix A.

In Fig. 6 are shown results of $\Delta q(n,k)$ estimated with some R_p and R_i values with a condition of $R_p + R_i = 1.01$; T_e and T_i are fixed to 1 and 300 μs, respectively. The oscillation in the curves of $\Delta q(n,k)$ results from the large time delay $T_i(\sim 350\ \mu s)$ caused by the drift of positive ions. In the condition of $R_p + R_i =$ constant, the oscillation becomes more intense with increasing R_i. It is also seen that $\Delta q(n,k)$ approaches to a single exponential, $\exp(\lambda t)$, of which the coefficient λ strongly depends on the combination of R_p and R_i; λ is larger as R_p increases in the condition of $R_p + R_i =$ constant.

The average current in each time interval T_i is given by

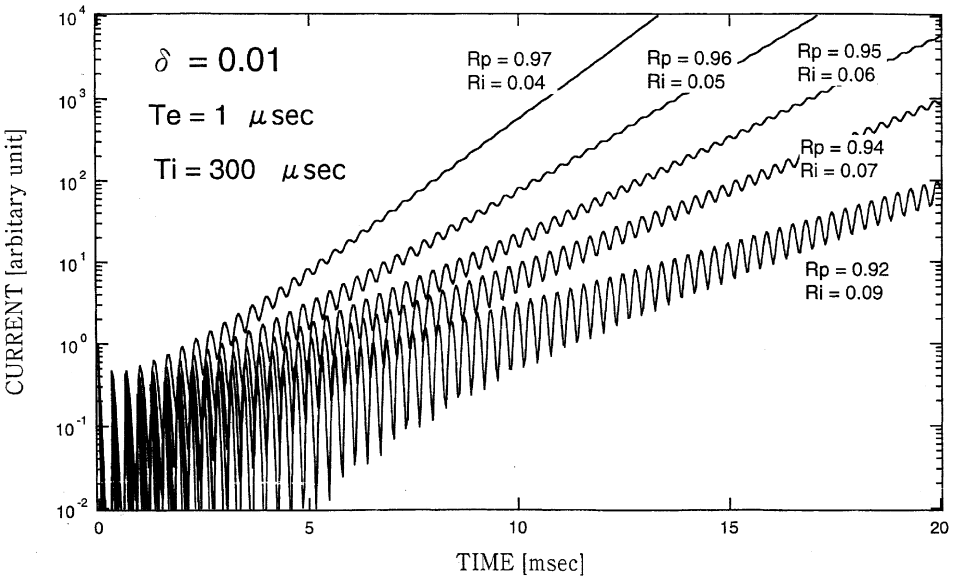

Fig. 6. Theoretical simulation for the current multiplication in the electric discharge obtained with various combinations of the parameters R_p and R_i; the sum of R_p and R_i is set to 1.01 in the simulation.

$$i_{\mathrm{av}}(n) = \sum_{k=0}^{N_\mathrm{i}} \frac{\Delta q(n,k)}{T_\mathrm{i}} = \frac{eG_0}{T_\mathrm{i}} \sum_{s=0}^{n} R_\mathrm{i}^s R_\mathrm{p}^{(n-s)N_\mathrm{i}} \sum_{k=0}^{N_\mathrm{i}} \binom{(n-s)N_\mathrm{i}+s+k}{s} R_\mathrm{p}^k. \tag{15}$$

when $R_\mathrm{p}^{N_\mathrm{i}} \sim 0$, $i_{\mathrm{av}}(n)$ is approximated as

$$i_{\mathrm{av}}(n) \sim \frac{eG_0}{T_\mathrm{i}} R_\mathrm{i}^n \sum_{k=0}^{\infty} \binom{n+k}{n} R_\mathrm{p}^k = \frac{eG_0}{T_\mathrm{i}} \frac{R_\mathrm{i}^n}{(1-R_\mathrm{p})^{n+1}}. \tag{16}$$

From this equation, an approximate form of the coefficient λ is derived as

$$\lambda = \frac{1}{T_\mathrm{i}} \ln\left(\frac{R_\mathrm{i}}{1-R_\mathrm{p}}\right). \tag{17}$$

5.2. Comparison with experimental results

In our previous work [10], the drift time of positive ions T_i and R_i defined by Eq. (3) was determined to be 320–380 and 0.088–0.307 μs, respectively, at 5–8 K, depending on the applied voltage. The drift time of electrons T_e is the order of 1 μs, but we have not a reliable value for T_e. Fixing T_i to 350 μs and R_i to 0.15, the coefficient λ for various R_p and T_e values has been estimated with Eq. (15). In Fig. 7 are given the results; the range of variables is 0.86–1.1 for R_p and 1.0–2.0 μs for T_e.

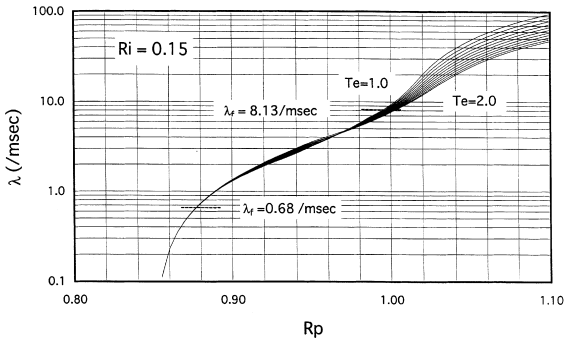

Fig. 7. Calculated results of the coefficient λ as function of R_p and T_e; other parameters R_i and T_i are fixed to 0.15 and 350 μs, respectively. Each curve corresponds to T_i values from 1.0 to 2.0 μs.

The experimental value of λ presently determined is 0.68 m s^{-1} for the slow component and 8.13 m s^{-1} for the fast component, as shown in Fig. 5. According to the estimation with Eq. (15), the R_p value corresponding to the slow component is 0.88 and that corresponding to the fast component is equal to or very near to unity. On the other hand, the R_i value is ~ 0.20, which has been deduced from the analysis of after-pulses observed at 4.2 K just before the electric discharge. These results indicates that, the contribution of the active photons to the electron multiplication process at 4.2 K is considerably larger than that of the positive ions.

6. Discussions

In addition to electron avalanches by electrons created in the primary ionization of incident radiations, avalanches by secondary electrons, which are produced by collisions of the active photons and the positive ions with cathode, also contribute to the output current in the proportional region of HFPC. Avalanches caused by the positive ions appear as the after-pulses in the output of charge-sensitive preamplifier. On the other hand, avalanches caused by the active photons overlap on avalanches by the primary ionization. In our previous works, the gas gain G was measured as a function of anode voltage, e.g., Fig. 5 in Ref. [10]. Now, it is clear that the quantity measured is not G but $G/(1-R_\mathrm{p})$, which contains the contribution from avalanches caused by the active photons. As long as R_p is measured independently, it is not possible to deduce a pure gas gain curve. One of the probable methods to obtain R_p as a function of anode voltage is to analyze the rise part of the output signal in the proportional operation. Thus, it is essentially important to know the R_p value for further understanding the counter operation of HFPC.

Many kinds of photons are emitted through various collision processes between electrons and helium atoms in electron avalanches. The active photons, which harm the counter operation, are

limited to a part of photons created by the collisions, as discussed below. A lot of highly-excited helium atoms He^* are produced by the collision of electron with normal helium $He(1^1s)$ in electron avalanches. One of decay channels for He^* is the de-excitation by collision with normal helium, in which He^* decays to low-lying excited states such as 2^1p, 2^3p, 2^1s and 2^3s or the ground state 1^1s. The other decay channel of He^* is radiative transitions. Non-resonance radiations are emitted through the decay to the low-lying excited states while resonance radiations are emitted through that to the ground state. Since resonance radiations are imprisoned in pure helium gas layer [15,16], they cannot reach to the cathode of HFPC. The probability for the decay of He^* by the emission of non-resonance radiations is much smaller than that by other processes, e.g., collisional de-excitations. Although the number of these radiations created in an avalanche is relatively small, their activities in the counter operation cannot be neglected. Without being absorbed by the helium gas layer, they can reach to the cathode and there emit photoelectrons; their energy is $0 \sim 4$ eV. There are the other channels to emit non-resonance radiations with higher energies (~ 10 eV) from the decay of excited molecular helium $He_2^*(A^1\Sigma_u^+)$ [17], which is produced by the collisional de-excitation of metastable $He^m(2^1s)$. However, the contribution of the photon from $He_2^*(A^1\Sigma_u^+)$ to the counter operation may be negligible because of its small photon emission rate at low temperatures.

It is now concluded that the active photons capable of harming the counter operation mainly consist of the non-resonance radiations emitted by the decay of He^* to low-lying excited states. Therefore, a cathode material with high work function such as nickel metal may be helpful to suppress the discharge in HFPC.

7. Concluding remarks

The current multiplication in electric discharge of HFPC is promoted by active particles created in the electron avalanche, i.e., non-resonance photons and positive helium ion clusters. The present analysis has revealed that $R_p(\sim 1)$ is much larger than $R_i(\sim 0.2)$, indicating that the non-resonance radiations play a main role in electric discharge. As shown in Section 4.4., the current multiplication in electric discharge takes place through two steps; the process is initiated as the slow component when $R(= R_p + R_i)$ is a little over unity, i.e., $R = 1.03$ in the present case, and then changes from slow to fast component with $R_p \sim 1$. However, the mechanism of the change has not been revealed in the present work. A further study for the electric discharge is clearly necessary.

It is expected that the counter operation and the electric discharge mainly depends on the amount of non-resonance photons created in an electron avalanche and the size of helium ion clusters at the cathode. These quantities are sensitively changed by both density and temperature of helium gas. We are planning a new experiment, in which both output and discharge signals from the preamplifier are examined as functions of gas density and temperature.

It is also desirable to understand the operation of HFPC and the discharge in it from the standpoint of atomic and molecular collision processes of helium. For this purpose, we are making a new model to describe the gas gain of proportional counter operation and the current multiplication in electric discharge using various data of collision processes in helium gas.

Appendix A. Theoretical curve of the electron multiplication in discharge

As illustrated in Fig. 8, the time t is divided into n blocks with an interval T_i and the residue $(t - nT_i)$ is further divided into k blocks with an interval T_e:

$$n \equiv \lfloor t/T_i \rfloor, \tag{A.1}$$

$$k = \lfloor (t - nT_i)/T_e \rfloor, \tag{A.2}$$

where $\lfloor X/x \rfloor$ means the integer part of the quotient X/x. In one time interval of T_i, the electron emission caused by the active photons repeats N_i times:

$$N_i = \lfloor T_i/T_e \rfloor. \tag{A.3}$$

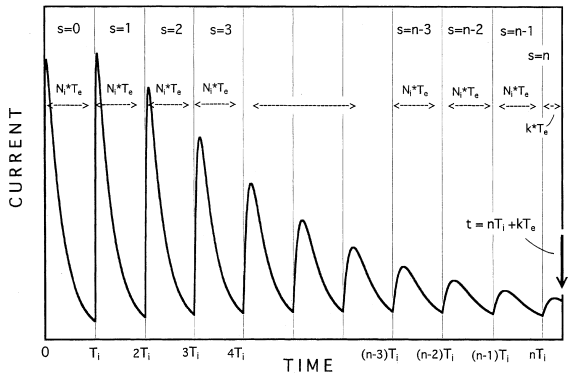

Fig. 8. An illustration for showing a procedure to deduce the theoretical curve of the electron multiplication in electric discharge.

Through the repeated electron emission by the photons, the charge eG_e, which appears at $t = 0$, generates new charges $\Delta q(0,k)$ at $t = nT_i + kT_e$

$$\Delta q(0,k) = eG_0 R_p^{nN_i+k} = \binom{nN_i + k}{0} R_p^{nN_i+k}. \quad (A.4)$$

In the second block $(n = 1)$ of $T_i \leqslant t < 2T_i$, the electron emission by the positive ions takes place after T_i after the emission by the photon in the first block $(n = 0)$ of $0 \leqslant t < T_i$. Each emission by the ions induces the successive emissions by the photons as similar to the case of the first block. The charge at $t = nT_i + kT_e$, which is generated by the emissions in the second block is expressed by

$$\Delta q(1,k) = eG_0 R_i R_p^{(n-1)N_i+k} \binom{(n-1)N_i + k + 1}{1}. \quad (A.5)$$

Similarly, the charge corresponding to the sth block is

$$\Delta q(s,k) = eG_0 R_i^s R_p^{(n-s)N_i+k} \binom{(n-s)N_i + k + s}{s}. \quad (A.6)$$

For the total charge at $t = nT_i + kT_e$, we obtain

$$\Delta Q(n,k) = eG_0 \sum_{s=0}^{n} \Delta q(s,k), \quad (A.7)$$

of which the explicit expression is given by Eq. (14) in the text.

References

[1] M.J. Tricker, in: J.G. Stevens, G.K. Shenoy (Eds.), Mössbauer Spectroscopy and its Chemical Applications, in: Advances in Chemistry Series no. 194, 1981.
[2] G. Balestrino, in: N.A. Eissa, G. Denardo (Eds.), Proceedings of the School on Applications of Nuclear Gamma Resonance Spectroscopy, World Scientific, Singapore, 1986, p. 159.
[3] G.N. Belozerski, Mössbauer Studies of Surface Layer, Elsevier, Amsterdam, 1993, p. 220.
[4] Y. Isozumi, T. Fujii, Current Topics in Crystal Growth Research, vol. 1, Research Trends, India, 1994, p. 187.
[5] Y. Isozumi, Y. Kishimoto, R. Katano, H. Takekoshi, Rev. Sci. Instr. 58 (1987) 293.
[6] Y. Isozumi, S. Ito, T. Fujii, R. Katano, Rev. Sci. Instr. 60 (1989) 3262.
[7] K. Fukumura, T. Kobayashi, A. Nakanishi, R. Katano, Y. Isozumi, Hyp. Int. 69 (1991) 755.
[8] S. Kishimoto, Y. Isozumi, R. Katano, H. Takekoshi, Nucl. Instr. and Meth. A 262 (1987) 755.
[9] S. Kishimoto, Y. Isozumi, Nucl. Instr. and Meth. A 286 (1990) 262.
[10] Y. Isozumi, R. Katano, S. Ito, S. Kishimoto, Nucl. Instr. and Meth. A 355 (1995) 443.
[11] A. von Engel, Ionized Gas, Clarendon, Oxford, 1965.
[12] H.D. Hagstrum, Phys. Rev. 96 (1954) 325.
[13] E. Kowalski, Nuclear Electronics, Springer, Berlin, 1970.
[14] Y. Isozumi, Nucl. Instr. and Meth. A 235 (1985) 164.
[15] T. Holstein, Phys. Rev. 72 (1947) 212.
[16] T. Holstein, Phys. Rev. 83 (1951) 1159.
[17] M.G. Payne et al., Phys. Rev. Lett. 35 (1975) 1154.